S41B-2186: A review of the virtual refraction and application to active source and regional imaging

T. Dylan Mikesell*, Kasper van Wijk* and Elmer Ruigrok†

*Physical Acoustics Lab and Department of Geosciences, Boise State University, 1910 University Dr., Boise, ID 83725
†Department of Geotechnology, Delft University of Technology, Stevinweg 1, 2628 CN, Delft, The Netherlands

Abstract

We present an overview of the spurious event in seismic interferometry called the virtual refraction. This artifact is present in the crosscorrelated wavefields when refractions are present in the raw data. We use this artifact to characterize the refractor velocity and a heterogeneous near-surface above the refractor. We formulate a *modified delay-time* statics method, which compared to the standard *delay-time* method, lacks a source static term. This is a direct result of using the virtual refraction as input rather than the real refraction. Finally, we present a regional-scale data example, wherein travel time perturbations are caused by mantle and crust heterogeneity. We crosscorrelate $\boldsymbol{P_{diff}}$ phases from many earthquakes. Then we remove the linear moveout associated with the virtual refraction along the core-mantle boundary. In this way, we estimate receiver-side traveltime anomalies in the western United States.

1. The virtual refraction

In field data applications of Seismic Interferometry (*Wapenaar and Fokkema*, 2006), an artifact related to head waves is present when the original data contain head waves (*Mikesell et al.*, 2009). This spurious event is called the *virtual refraction*. In the case of horizontal layers, the moveout of the virtual refraction defines the refractor velocity ($\boldsymbol{V_2}$).

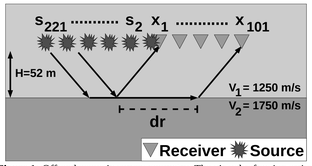

Figure 1: Off-end acoustic survey geometry. The virtual refraction arrival time is dr/V_2.

Figure 1 shows the geometry of an off-end acoustic numerical experiment. The shot record for a source at $\boldsymbol{X_1}$ is shown in Figure 2 (left). We crosscorrelate the wavefield at $\boldsymbol{X_1}$ with all other receivers and sum over each source, thus creating the virtual shot record in Figure 2 (right). Figure 3 demonstrates the stationary-phase points for the direct wave and virtual refraction.

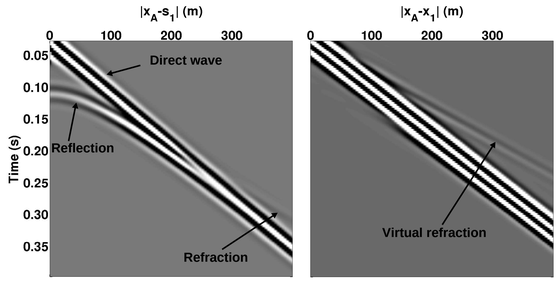

Figure 2: Real (left) and virtual (right) shot records for the off-end acoustic survey described in Figure 1. We taper the source array to zero on each end before summation. Therefore, stationary-phase points (*Snieder*, 2004) associated with the reflection are suppressed and we recover the direct wave and virtual refraction.

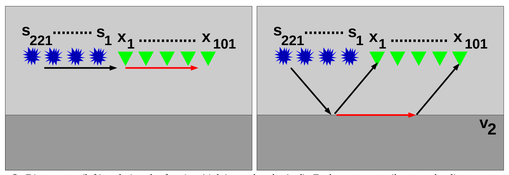

Figure 3: Direct wave (left) and virtual refraction (right) travel paths (red). Each source contributes to the direct wave and all sources past the critical offset contribute to the virtual refraction (*Mikesell et al.*, 2009).

2. Delay-time statics

Small traveltime perturbations (i.e., statics) due to near-surface heterogeneity deteriorate reflection seismic images. Figure 4 shows an example of a surface weathering layer that varies in thickness. A variety of methods exist to correct for this type of near-surface heterogeneity. For example, if the weathering layer velocity is known, elevation statics can be computed and the recorded seismic traces can be corrected.

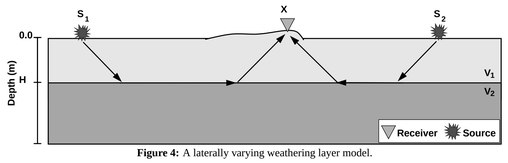

Figure 4: A laterally varying weathering layer model.

In areas where the weathering layer velocity is not known, other methods based on first-break analysis have been developed to estimate time shifts to correct for the source and receiver statics.

One such method is the *delay-time* method (e.g., p. 120 in *Burger et al.*, 2006). For a source on each side of $\boldsymbol{X}$ (Figure 4), we have two refraction travel-time equations:

$$T_{S_1X} = T_{S_1} + T_X + \frac{|S_1 - X|}{V_2}$$
$$T_{S_2X} = T_{S_2} + T_X + \frac{|S_2 - X|}{V_2}, \qquad (1)$$

where $|S_i - X|$ is the distance between the source (S_i) and receiver (X) and V_2 is the refractor velocity. T_{S_i} and T_X are delays associated with near-surface heterogeneity near the source or receiver, respectively.

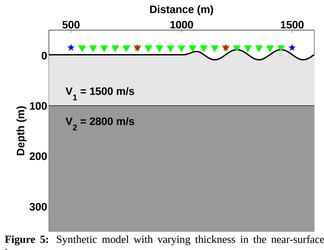

Figure 5: Synthetic model with varying thickness in the near-surface layer.

We test the *delay-time* method with a numerical 2D acoustic experiment using the Spectral Element Method (*Komatitsch and Vilotte*, 1998). On the left half of the model, the near-surface has a constant thickness of 100 m. On the right side, the near-surface thickness varies as a sine wave with a peak-to-peak variation of 20 m. We show the shot records from source $\boldsymbol{S_1}$ at 500 m distance (left) and $\boldsymbol{S_2}$ at 1500 m distance (right) in Figure 6. We use the modified-energy ratio (MER) method (*Han et al.*, 2008) to pick first breaks (red line).

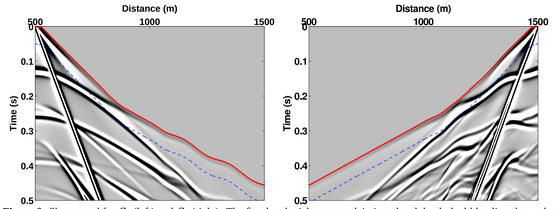

Figure 6: Shot record for $\boldsymbol{S_1}$ (left) and $\boldsymbol{S_2}$ (right). The first-break picks are overlain in red and the dashed-blue line shows the window of data used to estimate the virtual refraction.

We invert the system of travel-time equations to estimate each source static T_{S_i} and T_X (cyan line in Figure 9). We estimate each source static to be 105 ms and the refractor velocity V_2=2752 m/s. We estimate the model receiver static (blue line) relative to mean surface elevation (i.e., zero in this model). In the next section, we present a *modified delay-time* method that eliminates the source static estimate by incorporating the virtual refraction.

3. Modified statics with the virtual refraction

Consider two receivers at $\boldsymbol{X_A}$ and $\boldsymbol{X_B}$, crosscorrelating the refraction arrivals at $\boldsymbol{X_A}$ and $\boldsymbol{X_B}$ eliminates the shared parts of the raypath (T_S):

$$T_{SX_A} - T_{SX_B} = dT + \frac{|X_B - X_A|}{V_2}. \qquad (2)$$

The crosscorrelation represents the virtual refraction, plus the travel time perturbation, dT. dT is the receiver static at $\boldsymbol{X_A}$ relative to the reference receiver $\boldsymbol{X_B}$. The combination of the red raypaths in Figure 7 represent this crosscorrelation.

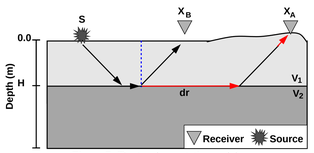

Figure 7: The two-layer statics model.

We crosscorrelate the receivers at the green stars in Figure 5 with every other receiver for each source (shown in Figure 8). However, before we crosscorrelate, we window around the first breaks (between red and dashed-blue lines in Figure 6). Therefore, we only crosscorrelate the direct wave or the refraction, and the first arrival becomes the virtual refraction rather than the direct wave. We apply the same inversion procedure for the modified arrival-time equations and virtual refraction first-break times.

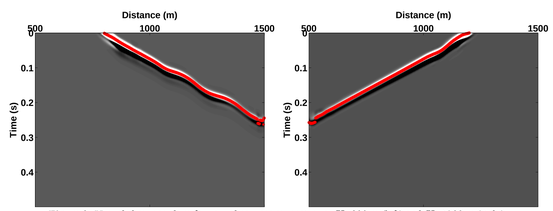

Figure 8: Virtual shot records at for virtual sources at receiver at $\boldsymbol{X}$=800 m (left) and $\boldsymbol{X}$=1200 m (right).

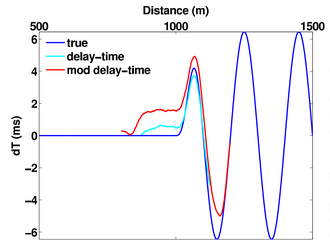

Figure 9: The *delay-time* (cyan) and *modified delay-time* (red) receiver statics. The true static relative to zero elevation is the blue line.

The receiver static is now estimated relative to the virtual source (i.e., $\boldsymbol{X}$=800 or 1200 m), which are both at the same elevation in this example. We plot the static estimated with the *modified delay-time* method in Figure 9 (red line). The refractor velocity estimated in this case is V_2=2731 m/s, a 2.5% underestimation. The extent of the usable refraction, illustrated in Figure 10, explains why the virtual refraction estimates receiver statics further in the lateral direction.

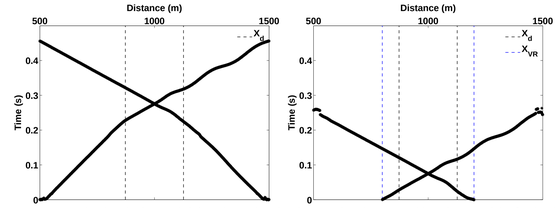

Figure 10: First break picks from real (left) and virtual (right) shot records. The increased lateral extent of the first break refraction explains the increase lateral resolution using the *modified delay-time* method.

4. Scanning for regional heterogeneity

The following examples show how we estimate travel-time anomalies within the crust and mantle below USArray. We use the $\boldsymbol{P_{diff}}$ crosscorrelations to isolate heterogeneity within the Earth. The $\boldsymbol{P_{diff}}$ raypaths between an earthquake (blue star) and an array of receivers (green triangles) are indicated in Figure 11. After applying crosscorrelation to $\boldsymbol{P_{diff}}$ arrivals, we take an average rayparameter of 4.62 s/deg and remove the far right term in equation 2. The retrieved anomalies (dT) using subarrays from USArray are shown in Figure 12. We extend the method to a larger section of USArray in Figures 13 and 14.

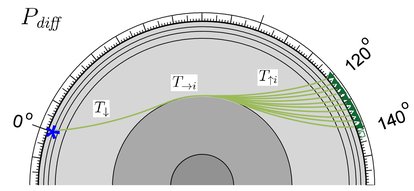

Figure 11: A 1D Earth model showing $\boldsymbol{P_{diff}}$ arrivals. The traveltime segments at the source-side, along the core-mantle boundary, and at the receiver-side are denoted with $T_\downarrow$, $T_{\rightarrow i}$ and $T_{\uparrow i}$, respectively, where i is a receiver index.

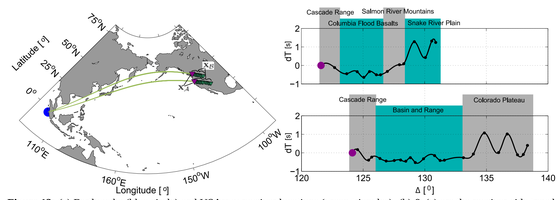

Figure 12: (a) Earthquake (blue circle) and USArray receiver locations (green triangles). (b) & (c) are the receiver-side travel-time anomalies (dT) for the northern and southern arrays, respectively. The points are the extracted anomalies at the different stations; the lines are created by spline interpolation.

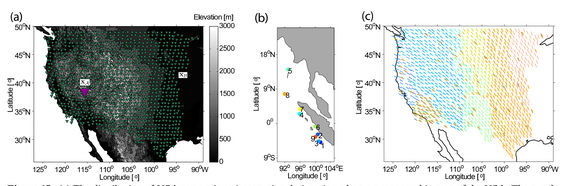

Figure 13: (a) The distribution of USArray stations (green triangles) projected onto a topographic map of the USA. The purple triangle at $\mathbf{X_A}$ indicates the reference station. (b) The locations of the 9 earthquakes used to make the anomaly map in Figure 14a. (c) Illumination map–the colored lines denote the backazimuth to the earthquakes in (b). In (b) and (c) the same colors are used.

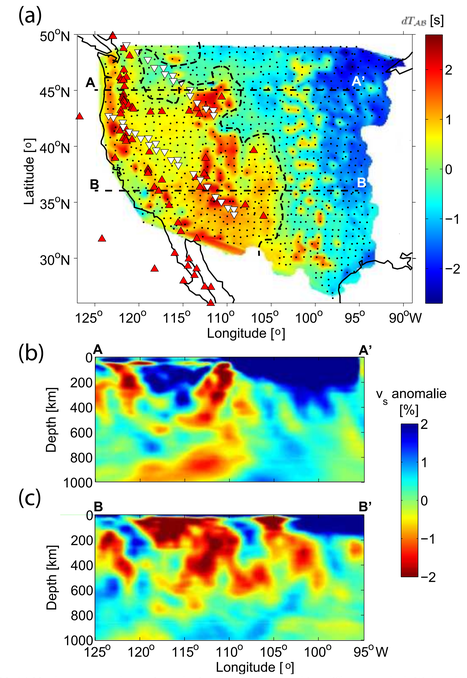

Figure 14: (a) Mantle-crust anomaly map imaged using the new $\boldsymbol{P_{diff}}$ traveltime-difference method. We have labeled 1) the primarily Holocene volcanism (red triangles, source: http://www.volcano.si.edu/); 2) the interpreted boundary between slow (west side) and fast (east side) lithosphere (undulating dashed line); 3) the location of two cross-sections A-A' and B-B' (dashed straight lines); 4) USArray stations used in this study (black dots); 5) the station locations used in Figure 12 (NE-SW subarrays of white triangles). (b) and (c) come from *Obrebski et al.* (2011) and are V_s anomaly sections along A-A' and B-B', respectively. These are extracted from the DNA10-S model (*Obrebski et al.*, 2011).

5. Conclusion

- For horizontal layers, we estimate the velocity of the faster layer from the slope of the virtual refraction.
- We estimate the refractor velocity and receiver statics using a modified *delay-time* inversion based on the virtual refraction, which increases the lateral resolution.
- We crosscorrelate CMB refractions ($\boldsymbol{P_{diff}}$) to isolate receiver-side heterogeneity within the crust & mantle.
- Traveltime delays in the Western USA seem to align with magmato-tectonic activity.
- High velocities in the East are likely related to Archean lithosphere and are under further investigation.

Acknowledgments

E.R is supported by The Netherlands Organization for Scientific Research (NWO). The facilities of the IRIS Data Management System, and specifically the IRIS Data Management Center, were used for access to waveform and metadata required in this study. Data from the TA network were made freely available as part of the EarthScope USArray facility supported by the National Science Foundation, Major Research Facility program under Cooperative Agreement EAR-0350030. We thank the developers of SPECFEM2D numerical modeling software.

References

Burger, H. R., A. F. Sheehan, and C. H. Jones (2006), *Introduction to Applied Geophysics: Exploring the Shallow Subsurface*, W. W. Norton & Company.

Han, L., J. Wong, J. C. Bancroft, and R. R. Stewart (2008), Automatic time picking and velocity determination on full waveform sonic well logs, *Tech. Rep. 20*, CREWES, University fo Calgary.

Komatitsch, D., and J.-P. Vilotte (1998), The spectral element method: An efficient tool to simulate the seismic response of 2d and 3d geological structures, *Bull. Seism. Soc. Am.*, *88*(2), 368–392.

Mikesell, D., K. van Wijk, A. Calvert, and M. Haney (2009), The virtual refraction: Useful spurious energy in seismic interferometry, *Geophysics*, *74*(3), A13–A17, doi:10.1190/1.3095659.

Obrebski, M., R. M. Allen, F. Pollitz, and S. Hung (2011), Lithosphere-asthenosphere interaction beneath the western United States from the joint inversion of body-wave traveltimes and surface-wave phase velocities, *Geophysical Journal International*, *185*(2), 1003–1021, doi: 10.1111/j.1365-246X.2011.04990.x.

Snieder, R. (2004), Extracting the Green's function from the correlation of coda waves: A derivation based on stationary phase, *Phys. Rev. E*, *69*(4), 046,610, doi: 10.1103/PhysRevE.69.046610.

Wapenaar, K., and J. Fokkema (2006), Green's function representations for seismic interferometry, *Geophysics*, *71*(4), S133–S146, doi:10.1190/1.2213955.

author email: dmikesell@cgiss.boisestate.edu **AGU FALL MEETING 2011**